

LightFuse: Lightweight CNN based Dual-exposure Fusion

Ziyi Liu¹, Jie Yang², and Orly Yadid-Pecht, *Fellow, IEEE*¹

¹I2Sense lab, University of Calgary, Calgary T2N 1N4, Canada

²Westlake University, Hangzhou 310024, China

Abstract—Deep convolutional neural networks (DCNN) aided high dynamic range (HDR) imaging recently received a lot of attention. The quality of DCNN generated HDR images have overperformed the traditional counterparts. However, DCNN is prone to be computationally intensive and power-hungry. To address the challenge, we propose LightFuse, a light-weight CNN-based algorithm for extreme dual-exposure image fusion, which can be implemented on various embedded computing platforms with limited power and hardware resources. Two sub-networks are utilized: a *GlobalNet* (G) and a *DetailNet* (D). The goal of G is to learn the global illumination information on the spatial dimension, whereas D aims to enhance local details on the channel dimension. Both G and D are based solely on depthwise convolution (D_Conv) and pointwise convolution (P_Conv) to reduce required parameters and computations. Experimental results display that the proposed technique could generate HDR images with plausible details in extremely exposed regions. Our PSNR score exceeds the other state-of-the-art approaches by 1.2 to 1.6 times and achieves 1.4 to 20 times FLOP and parameter reduction compared with others¹.

Index Terms—Multi-exposure fusion, High dynamic range image, Deep learning, Light-weight neural network, CNN.

I. INTRODUCTION

The dynamic range is defined as the ratio of the intensity of the brightest point to that of the darkest point in a scene or an image. In the real-world, the dynamic range is extremely broad from 0 to 1,000,000. The human visual system (HVS) can perceive a range of around 24 exposure value (EV) [1] at one time. Nevertheless, conventional digital cameras can only capture a range of approximately 9 EV. The dynamic range of digital images is mainly determined by the saturation current of the photoelectric response and dark current of the imaging device. The dynamic range of each device is fixed and usually cannot match the dynamic range of the natural scene, leading to overexposed or underexposed images that miss details in the brightest or the darkest regions. High dynamic range (HDR) imaging technology is used to overcome this deficiency in modern cameras. HDR images can show rich appearances of natural scenes such as lighting, contrast, and details and are extremely important in many applications such as photography, autonomous vehicles [2]. Some professional hardware devices have been devised to capture high dynamic range [3], [4]. However, these devices are either expensive or

bulky. Researchers are resolving this issue on the algorithmic level and designed plethoric algorithms to reproduce a greater range of luminosity. The most popular algorithm to generate an HDR image is known as multi-exposure fusion (MEF) [5]. It merges a sequential low dynamic range (LDR) image with different exposure to display more details.

In general, MEF methods can be classified into traditional and deep learning-based (DL) MEF methods. Traditional MEF methods [6]–[8] manually design mathematical transformation and fusion equations and apply the functions on the image bracket for blending multiple exposures of the same scene into a single image. However, it is hard to design appropriate equations manually to pick the important features from each input image. DL approaches are more likely to avoid this problem because the trained neural networks (NNs) can automatically generate the complex relationship between source images and fused images. Wu et al. [9] designed the first non-flow-based deep framework with a model size of 64MB. Kalantari et al. [10] used a convolutional neural network (CNN) as their learning model and presented three different architectures for MEF, the model needs 4.08 MB memory. Among these methods, classical CNNs as a preferred network structure have issues such as extravagant power consumption, excessive parameters, and heavy computation resources occupation, making them hard to deploy on embedded computing applications. Commonly, CNN methods are implemented on the “cloud” to provide sufficient computing resources [11]. However, cloud computing risks the safety of the user privacy and introduces data transceiving delays that are critical to many real-time applications such as driverless cars [12], security surveillance [13], and industrial automation [14]. Running a DL model on local devices can avoid delays, security, and privacy vulnerabilities, but also introduces new challenges to design lightweight model for power and resource-constrained devices. This paper presents LightFuse, the first lightweight image fusion model, to our best knowledge. It consists of two different networks *GlobalNet* and *DetailNet*, finds the global- and local-related patterns separately to prevent high-computational cost, and eludes underfitting through mimicking the process procedure of standard convolutions.

The organization of this paper is as follows. We describe our proposed dual-exposure fusion algorithm in section 2, and compare it with the most state-of-the-art methods in section 3. At last, we conclude the paper in section 4.

Corresponding author: J. Yang (email: yangjie@westlake.edu.cn).

¹The code is made publicly available at <https://github.com/Taichi-Pink/LightFuse-Lightweight-CNN-based-Dual-exposure-Fusion>

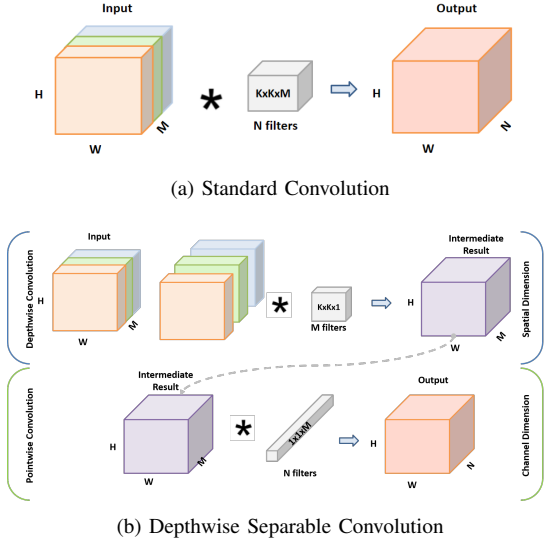


Fig. 1: The standard convolution in (a) is replaced by two stages: depthwise convolution and pointwise convolution in (b) to build a depthwise separable convolution.

Input Size	Operator	Output Size
$W \times H \times 6$	Separable Conv 3x3	$W \times H \times 256$
$W \times H \times 256$	Separable Conv 3x3	$W \times H \times 64$
$W \times H \times 64$	Separable Conv 3x3	$W \times H \times 3$

TABLE I: T_CNN architecture based on depthwise separable convolution

II. ARCHITECTURE

The architecture of lightweight is shown in Fig. 2. It takes extreme overexposure and underexposure images as input. A *GlobalNet* is utilized to extract the global structural information of the input images on the spatial dimension, and a *DetailNet* is adopted to enhance local details on the channel dimension.

A. Trial Convolutional Neural Network

Table I illustrates a trial CNN (T_CNN) architecture, consisting of three depthwise separable convolution (DS_Conv) layers. The creation of DS_Conv [15]–[17] is motivated by optimizing the standard convolution process by separating the process into two stages. More precisely, the computational cost is greatly reduced when a conventional convolution is replaced with two sub-tasks, a depthwise convolution (D_Conv) and a pointwise convolution (P_Conv). As shown in Fig. 1a, the standard convolution tries to learn features from three-dimension, dealing with both spatial dimensions and a depth dimension. Differently, in Fig. 1b, a DS_Conv initially performs a spatial convolutional calculations with $K \times K$ kernels. Then standard 1×1 convolutions are applied to integrate information for all channels.

From Fig. 3, we can see that DS_Conv structure has the potential to extract and reconstruct desirable information from differently exposed images. We enhance the T_CNN by

creating and training two separate networks (Fig. 2), one that focuses on the channel dimension and the other operates on the spatial dimension. By separating the channel and spatial dimensions into separate networks, we avoid the problem of the original proposed T_CNN , which alternately trains on the spatial and channel dimensions.

B. Overall architecture

Most MEF algorithms [9], [18]–[20] need a sequence of LDR images to generate high-quality HDR images, hence these algorithms require many LDR images to capture the whole dynamic range of the scene, causing problems such as large storage requirements, processing time, and power budget. However, the exposure difference between successive LDR images in the exposure stack is slight, causing information redundancy. In our architecture, we only utilize two extremely exposed images with complementary information, together they contain all the information necessary for image fusion. As shown in Fig. 4, each image contains relevant information that is not present in the other image.

The *GlobalNet* (G) has a U-net-shaped [21] structure, made up of an encoder-decoder. The encoder consists of 3 different convolution layers, which perform a subsequent down-sampling operation on their respective inputs, while the decoder contains 3 up-sampling layers to reconstruct the compressed representation. In the encoder, the number of channels of the first two D_Conv with strides of two stays the same as 6 until the third DS_Conv sets it as 3 in correspondence with the final outputs. However, this network only filters the input channel to capture the higher-level global information, it does not combine them to create new features. *DetailNet* (D) focuses on the channel dimension, by projecting the input channel onto a large channel space, and learns new features from the high-dimensional space. The model consists of three P_Conv layers, each followed by a ReLU layer. The number of channels is increased from 6 to 256 through the first layer to expand the channel space, and then decreased to 64 and 3 through the following two layers to combine channel-related information. We adopt 1×1 kernels to maintain detailed information and ensure that no crucial information is missed. The last layer of *LightFuse* is an add layer that merges the learned global and local information from two sub-nets, followed by a Tanh activation function.

We display the effect of two sub-nets in Fig. 5, from which it demonstrates that G only has access to global illumination information and D is sensitive to local details. For example, G compresses inputs and saves the large gradients, which are generally the contours of objects (Fig. 5a). On the contrary, D fuses the information from two inputs and enhances the local details as shown in Fig. 5b. The critical reasons for the distinct functions of the two sub-nets are the differences in channels and kernel size. G has a larger kernel size; thus, it can receive a broader receptive field [22] and focus on global features. On the other hand, D with 1×1 kernels expands channel space and extracts fine-grained local features to describe the local structure of the image contents.

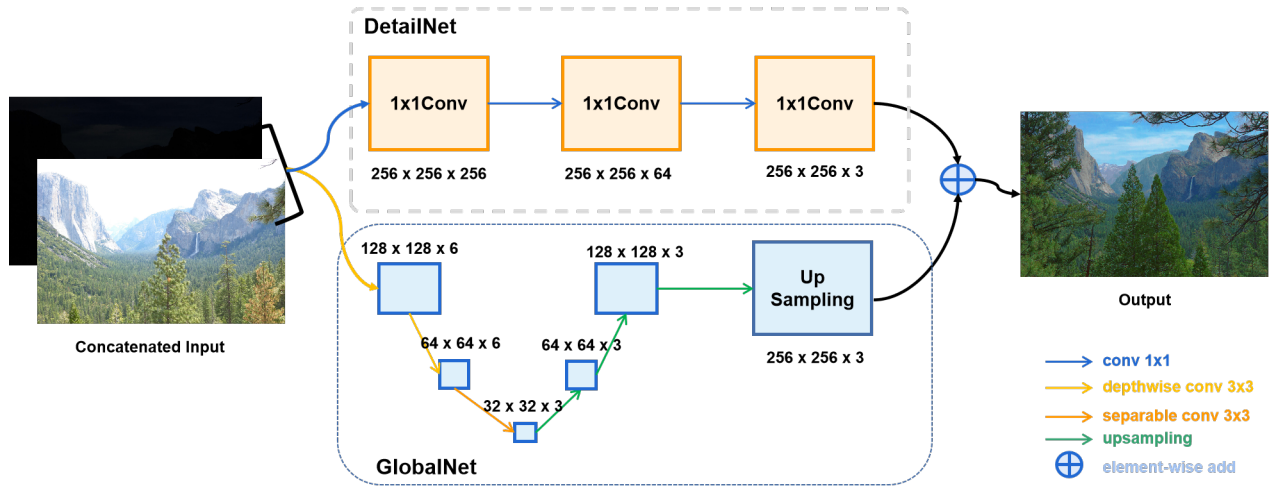


Fig. 2: An overview of our lightweight image fusion method. Our proposed method comprises two networks: a *GlobalNet* and a *DetailNet*. Given extreme overexposure and underexposure images as inputs, the *GlobalNet* extracts the global illumination information, while the *DetailNet* enhances the local details. Eventually, the output image is obtained by adding the features obtained from the two sub-nets, followed by a Tanh operation.

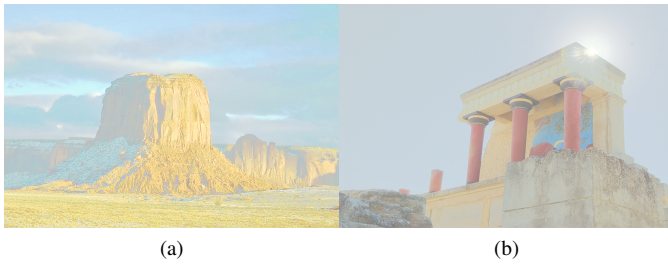


Fig. 3: Obtained HDR through T_CNN architecture.

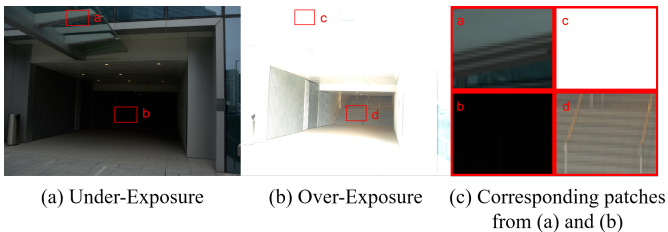


Fig. 4: Under- and over-exposed input.



Fig. 5: Compare image gradients from two sub-nets

C. Loss Function

To train the network, a combination of two different loss functions are used: perceptual loss [23] and mean square error loss (MSE). Perceptual loss compares high-level abstractions

between the generated image and the ground truth by passing these two through a pre-trained network that applies convolution layers to extract features and patterns, and calculates the distance between the generated image and its ground truth.

$$L_{perceptual} = \sum_i \| f_i(I_{out}) - f_i(I_{label}) \|_1 \quad (1)$$

In our work, VGG19 [24] is chosen as the feature extractor noted as f in Equation 1, and I_{out} and I_{label} represent the network output and ground truth image.

$$L_{mse} = \frac{1}{n} \sum_{j=1}^n (I_{out_j} - I_{label_j})^2 \quad (2)$$

The MSE loss function is given above. Here n refers to the number of pixels in I_{out} or I_{label} . It is used as a metric for understanding differences between images on a pixel by pixel level.

$$L = L_{perceptual} + L_{mse} \quad (3)$$

Our training function is defined in Equation 3, a mixture of two different loss functions.

D. Implementation Details

We use Adam as the optimizer and set the learning rate and batch size as 0.001 and 20 apart. Although deeper models empirically achieve better performance, we aim to present a simple idea as a reference in the high dynamic range image field. The overall framework can be written in Keras [25] or other high-level neural network libraries, and it takes around 15 lines of code. The range of values of training data and labels is all from -1 to 1.

III. EXPERIMENT AND EVALUATION

A. Dataset

We take SICE dataset [26] for training and testing the proposed network. The dataset² contains two parts; in this paper, we only use the first part with 360 sequences, because the first part has more classic pictures the authors obtained from a widely used dataset [27]. We randomly select 80% images for training and use the remaining 20% for testing. For the sake of carrying out practical training, we crop the original full-size image into 256×256 patches with a stride of 256, generating about 68,000 patches.

B. Evaluation and Comparison

We compare LightFuse with previous MEF methods, including Mertens09 [18], DeepFuse [28], and MEF-Net [29]. Mertens09 is the primary baseline in MEF. DeepFuse is a closely related method that trains a convolutional network for dual-exposure image fusion. MEF-Net is a fast method by weight fusion.

Qualitative Comparison. As shown in scenes 1, 4 of Fig. 6, Mertens09 tends to be dark, as their pyramid reconstruction cannot guarantee the produced intensities within the range from 0 to 1. DeepFuse contains too much brightness and leads to over-contrast, such as the region in scene 1 where the sky meets the mountain. Our operation exhibits the scenes more visually pleasing, e.g., the mountain is presented clearly, the sky is bluer than reference, and the sharpness of the forest is preserved, while Mertens09 performs poorly in general at overexposed regions and DeepFuse can only partially recover the details. In scene 2, where the proposed method outperforms others in highlight regions, Mertens09 fails to recover the details of the lamp due to the extreme dynamic range of the scene and excessive gaussian smoothing of the weight maps. The white flowers in scene 3 are displayed obviously in LightFuse, however, those details from others are over-saturated and cannot be exhibited as expected. Therefore, LightFuse produces a more natural appearance with faithful details and color reproductions.

Quantitative and Computational Complexity Comparison. We list the quantitative comparison results in terms of peak signal to noise ratio (PSNR) and structural similarity index measure (SSIM) in Table II. PSNR measures the distortion by the ratio of peak value power and noise power; SSIM is well correlated with HVS and designed based on three factors: brightness, contrast, and structure. In Table II, the DL methods DeepFuse [28] and ours have surpassed the traditional one Mertens09 [18] because the DL model is trained on a preprocessed dataset, where the model discovers the underlying patterns in images and automatically works out the most descriptive and salient features concerning each exposure of a scene. However, the performance of MEF-Net [29] is not competitive because MEF-Net prefers three or more exposure inputs. The testing platform is a computer with an Intel i7-8565U (1.8GHz) CPU and GeForce RTX 2080

²<https://github.com/csjscai/SICE>

Algorithm	PSNR	SSIM
MEF-Net [29]	11.5010	0.6732
Mertens09 [18]	15.4731	0.7565
DeepFuse [28]	17.1632	0.7669
Ours	18.9538	0.7908

TABLE II: Average PSNR and SSIM scores. The cells containing highest score across all scenes are highlighted in bold.

Algorithm	FLOPs	Parameters	Exe. Times (sec)
DeepFuse [28]	$W \times H \times 736,928$	369,921	202.0535
MEF-Net [29]	$W \times H \times 52,320$	26,305	0.6781
Ours(CPU)	$W \times H \times \mathbf{36,260}$	18,630	0.1425
Ours(GPU)	$W \times H \times \mathbf{36,260}$	18,630	0.0646

TABLE III: Comparison of computation complexity.

Ti GPU. Mertens09 [18], DeepFuse [28], and MEF-Net [29] utilize CPU, while LightFuse exploits CPU and GPU.

We conduct a computational complexity comparison as to the number of floating point operations (FLOPs) and parameters. The computational cost of Deepfuse [28] and MEF-Net [29] is 20x and 1.4x larger than ours, as shown in Table. III. Meanwhile, the total number of parameters of DeepFuse and MEF-Net is around 20x and 1.4x more as well. Compared with DeepFuse and MEF-Net on the same resolution, our method is 1418x and 4.8x more rapid.

IV. CONCLUSION AND FUTURE WORK

In this paper, we propose a lightweight network for image fusion. Come from the rationale of depthwise separable convolution, we suggest an exposure fusion framework LightFuse that is composed of two sub-nets, where *GlobalNet* focuses on the global illumination information and *DetailNet* aims to improve local details. This particular architecture reduces the size and latency without sacrificing prediction accuracy. Our method may bring benefits to deploy deep learning architectures on hardware accelerators in the near future, for which we often consider the issue of hardware utilization. Under limited resources, the support of hardware for any operation requires hardware resources preoccupied. Therefore, we desire methods that greatly alleviate this problem and achieve a trade-off between hardware flexibility and computing performance.

REFERENCES

- [1] S. F. Ray, "Camera exposure determination," *The manual of photography: Photographic and digital imaging*, vol. 2, 2000.
- [2] N. Paul and C. Chung, "Application of hdr algorithms to solve direct sunlight problems when autonomous vehicles using machine vision systems are driving into sun," *Computers in Industry*, vol. 98, pp. 192–196, 2018.
- [3] M. D. Tocci, C. Kiser, N. Tocci, and P. Sen, "A versatile hdr video production system," *ACM Transactions on Graphics (TOG)*, vol. 30, no. 4, pp. 1–10, 2011.
- [4] S. K. Nayar and T. Mitsunaga, "High dynamic range imaging: Spatially varying pixel exposures," in *Proceedings IEEE Conference on Computer Vision and Pattern Recognition. CVPR 2000 (Cat. No. PR00662)*, vol. 1. IEEE, 2000, pp. 472–479.

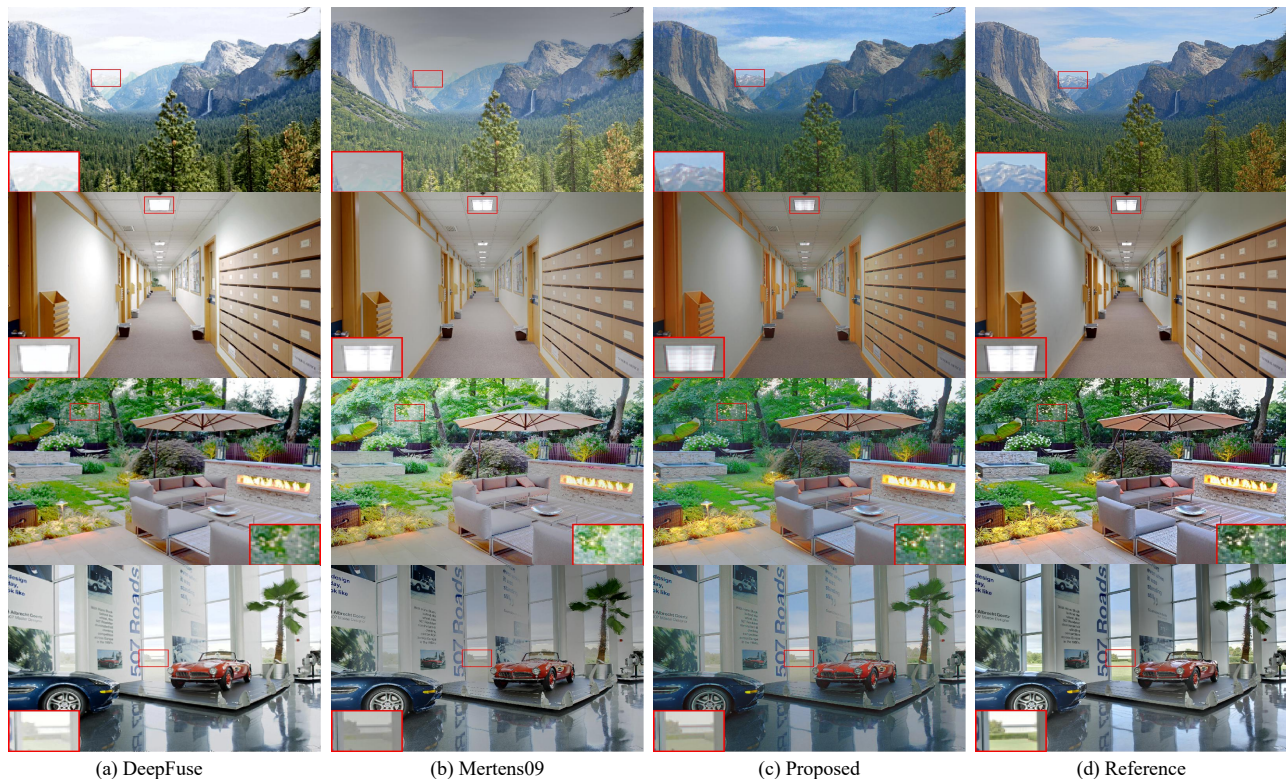


Fig. 6: Comparative results of our LightFuse with DeepFuse [28] and Mertens09 [18].

- [5] T. Mertens, J. Kautz, and F. Van Reeth, "Exposure fusion," in *15th Pacific Conference on Computer Graphics and Applications (PG'07)*. IEEE, 2007, pp. 382–390.
- [6] S. Li, X. Kang, and J. Hu, "Image fusion with guided filtering," *IEEE Transactions on Image Processing*, vol. 22, no. 7, pp. 2864–2875, 2013.
- [7] K. Ma, H. Li, H. Yong, Z. Wang, D. Meng, and L. Zhang, "Robust multi-exposure image fusion: a structural patch decomposition approach," *IEEE Transactions on Image Processing*, vol. 26, no. 5, pp. 2519–2532, 2017.
- [8] K. Ma, Z. Duanmu, H. Yeganeh, and Z. Wang, "Multi-exposure image fusion by optimizing a structural similarity index," *IEEE Transactions on Computational Imaging*, vol. 4, no. 1, pp. 60–72, 2017.
- [9] S. Wu, J. Xu, Y.-W. Tai, and C.-K. Tang, "Deep high dynamic range imaging with large foreground motions," in *Proceedings of the European Conference on Computer Vision (ECCV)*, 2018, pp. 117–132.
- [10] N. K. Kalantari and R. Ramamoorthi, "Deep high dynamic range imaging of dynamic scenes," *ACM Trans. Graph.*, vol. 36, no. 4, pp. 144–1, 2017.
- [11] J. Wang, B. Cao, P. Yu, L. Sun, W. Bao, and X. Zhu, "Deep learning towards mobile applications," in *2018 IEEE 38th International Conference on Distributed Computing Systems (ICDCS)*. IEEE, 2018, pp. 1385–1393.
- [12] S. Liu, L. Liu, J. Tang, B. Yu, Y. Wang, and W. Shi, "Edge computing for autonomous driving: Opportunities and challenges," *Proceedings of the IEEE*, vol. 107, no. 8, pp. 1697–1716, 2019.
- [13] S. Y. Nikouei, Y. Chen, S. Song, R. Xu, B.-Y. Choi, and T. Faughnan, "Smart surveillance as an edge network service: From harr-cascade, svm to a lightweight cnn," in *2018 IEEE 4th international conference on collaboration and internet computing (cic)*. IEEE, 2018, pp. 256–265.
- [14] L. Li, K. Ota, and M. Dong, "Deep learning for smart industry: Efficient manufacture inspection system with fog computing," *IEEE Transactions on Industrial Informatics*, vol. 14, no. 10, pp. 4665–4673, 2018.
- [15] F. Chollet, "Xception: Deep learning with depthwise separable convolutions," in *Proceedings of the IEEE conference on computer vision and pattern recognition*, 2017, pp. 1251–1258.
- [16] A. G. Howard, M. Zhu, B. Chen, D. Kalenichenko, W. Wang, T. Weyand, M. Andreetto, and H. Adam, "Mobilenets: Efficient convolutional neural networks for mobile vision applications," *arXiv preprint arXiv:1704.04861*, 2017.
- [17] M. Sandler, A. Howard, M. Zhu, A. Zhmoginov, and L.-C. Chen, "Mobilenetv2: Inverted residuals and linear bottlenecks," in *Proceedings of the IEEE conference on computer vision and pattern recognition*, 2018, pp. 4510–4520.
- [18] T. Mertens, J. Kautz, and F. Van Reeth, "Exposure fusion: A simple and practical alternative to high dynamic range photography," in *Computer graphics forum*, vol. 28, no. 1. Wiley Online Library, 2009, pp. 161–171.
- [19] S. Li and X. Kang, "Fast multi-exposure image fusion with median filter and recursive filter," *IEEE Transactions on Consumer Electronics*, vol. 58, no. 2, pp. 626–632, 2012.
- [20] Y. Niu, J. Wu, W. Liu, W. Guo, and R. W. Lau, "Hdr-gan: Hdr image reconstruction from multi-exposed ldr images with large motions," *IEEE Transactions on Image Processing*, vol. 30, pp. 3885–3896, 2021.
- [21] O. Ronneberger, P. Fischer, and T. Brox, "U-net: Convolutional networks for biomedical image segmentation," in *International Conference on Medical image computing and computer-assisted intervention*. Springer, 2015, pp. 234–241.
- [22] W. Luo, Y. Li, R. Urtasun, and R. Zemel, "Understanding the effective receptive field in deep convolutional neural networks," 2017.
- [23] J. Johnson, A. Alahi, and L. Fei-Fei, "Perceptual losses for real-time style transfer and super-resolution," in *European conference on computer vision*. Springer, 2016, pp. 694–711.
- [24] K. Simonyan and A. Zisserman, "Very deep convolutional networks for large-scale image recognition," *arXiv preprint arXiv:1409.1556*, 2014.
- [25] F. Chollet, "keras," <https://github.com/fchollet/keras>, 2015.
- [26] J. Cai, S. Gu, and L. Zhang, "Learning a deep single image contrast enhancer from multi-exposure images," *IEEE Transactions on Image Processing*, vol. 27, no. 4, pp. 2049–2062, 2018.
- [27] H. Nemoto, P. Korshunov, P. Hanhart, and T. Ebrahimi, "Visual attention in ldr and hdr images," in *9th International Workshop on Video Processing and Quality Metrics for Consumer Electronics (VPQM)*, no. CONF, 2015.
- [28] K. R. Prabhakar, V. S. Srikar, and R. V. Babu, "Deepfuse: A deep unsupervised approach for exposure fusion with extreme exposure image pairs," in *ICCV*, vol. 1, no. 2, 2017, p. 3.
- [29] K. Ma, Z. Duanmu, H. Zhu, Y. Fang, and Z. Wang, "Deep guided learning for fast multi-exposure image fusion," *IEEE Transactions on Image Processing*, vol. 29, pp. 2808–2819, 2019.